Catalysis Today 426 (2024) 114386

Contents lists available at ScienceDirect

Catalysis Today

journal homepage: www.elsevier.com/locate/cattod

Experimental investigation and 2D mathematical modelling of copper foams packed with Rh-Al_2O_3 catalysts for the intensification of methane steam reforming

Giulia Ferri, Matteo Ambrosetti, Alessandra Beretta, Gianpiero Groppi, Enrico Tronconi *

Laboratory of Catalysis and Catalytic Processes (LCCP), Dipartimento di Energia, Politecnico di Milano, Via La Masa 34, 20156 Milano, Italy

ARTICLE INFO

Keywords:
Hydrogen production
Structured catalysts
Process intensification

ABSTRACT

Efficient heat transfer is a crucial factor in the design of compact methane steam reformers for delocalized hydrogen production. The use of copper packed foams was proposed few years ago by our group to strongly intensify heat transfer in these systems, allowing the design of small-scale units with minimal radial temperature gradients. In this study, a new experimental campaign was performed to demonstrate the concept potential under industrially relevant heat fluxes and to establish an experimental foundation for validating a 2D mathematical model of the process. Copper open-cell foams were packed with a Rh/Al_2O_3 egg-shell catalyst and loaded into a 29.5 mm diameter tubular reactor, which was heated using a lab-scale oven. By leveraging the combined benefits of enhanced heat transfer, granted by the copper foam, and the high activity of the Rh-based eggshell catalyst, experiments were successfully performed at gas hourly space velocities (GHSV) ranging from 10 to 30 $Nm^3/h/kg_{cat}$, with heat duties of up to 9 MW/m^3. These experiments lead to a methane conversion close to thermodynamic equilibrium while maintaining limited radial gradients within the system (maximum 20 °C across the mid-radius). A predictive pseudo-heterogeneous 2D reactor model was developed and validated against experimental data. The model accurately captured the observed trends in temperature profiles and outlet concentrations, and can be utilized for optimized design, paving the way for the development of efficient small-scale hydrogen production units.

1. Introduction

Since the beginning of 19th century, chemical industries have developed technologies for producing hydrogen, a key molecule for the upgrade of hydrocarbons and for methanol and ammonia synthesis [1]. Until recently, hydrogen uses were mainly concentrated in the chemical and petrochemical sectors, where processes typically take advantage of the economy of scale. Indeed, the technological development led to the design of processes, such as autothermal reforming or externally fired hydrocarbons reforming (mainly methane) suited to produce syngas and hydrogen at flowrates up to 200.000 Nm^3/h [2]. The consolidated technologies employed to these aims are methane autothermal reforming and methane steam reforming.

Autothermal reforming is an adiabatic process where hydrocarbons are mixed with oxygen and water. In the first portion of the reactor, combustion reaction takes place and releases a significant amount of heat, that sustains the endothermic reforming reaction taking place in the catalytic section of the reactor.

Steam reforming is instead an endothermic process where hydrocarbons react with H_2O. To sustain the reaction, the same hydrocarbon or other available fuel gases are burned in air and the heat is transferred to the reactor tubes with a radiative/convective mechanism. The reaction is conventionally catalyzed with commercial Nickel catalyst pellets, that are loaded in a bundle of tubes, which are typically 8–15 m long and 8–20 cm in diameter to keep high gas velocity and reasonable specific heat exchange areas. When natural gas is employed, the process is typically operated at pressures of 20–30 bar and outer tube temperatures of about 900 °C to ensure adequate conversion levels [2]. The process is well established and has reached a high level of optimization, both in terms of thermal integration and in terms of efficiency of unit operations. In particular, the heat transfer efficiency in the reforming section is granted by very strong convective heat transfer promoted by suitable tube and pellet geometries.

In the last decades, however, the rising warnings associated with climate changes require new paradigms towards energy uses in

* Corresponding author.
E-mail address: enrico.tronconi@polimi.it (E. Tronconi).

https://doi.org/10.1016/j.cattod.2023.114386
Received 13 July 2023; Received in revised form 8 September 2023; Accepted 15 September 2023
Available online 19 September 2023

Nomenclature

CI	Catalyst loading [kg_{cat}/m^3]
cp_{mix}	Specific heat [J/kg/K]
d_{cell}	Foam cell diameter [mm]
D_{eff}	Effective diffusion coefficient [m^2/s]
h_{pf}	Interphase heat transfer coefficient [$W/m^2/K$]
h_w	Wall-pseudo-phase heat transfer coefficient [$W/m^2/K$]
h_{wf}	Wall-foam heat transfer coefficient [$W/m^2/K$]
GHSV	Gas hourly space velocity [$Nm^3/kg_{cat}/h$]
G	Specific mass flowrate [$kg/m^2/s$]
k_p	Pseudo-phase conductivity [W/m/K]
k_f	Foam conductivity [W/m/K]
MW_i	Molar weight [kg/mol]
P	Pressure [atm]
r	Radial coordinate [m]
r_j	Reaction rate [$mol/g_{cat}/s$]
S_v	Specific surface area [1/m]
T_f	Foam temperature [K]
T_{fur}	Furnace temperature [K]
T_p	Pseudo-phase temperature [K]
T_W	Wall temperature [K]
$U_{overall}$	Global heat exchange coefficient [$W/m^2/K$]
v	Velocity [m/s]
z	Axial coordinate [m]
$\Delta H_{reaz\,j}$	Reaction enthalpy [J/mol]
ε_{foam}	Foam void fraction
η_j	Effectiveness factor
ν_{ij}	Stoichiometric coefficient
μ	Dynamic viscosity [kg/m/s]
ρ_{mix}	Density [kg/m^3]
ω_i	Mass fraction

industrial and domestic sectors with challenging tasks in terms of reduction of CO_2 emissions. Hydrogen, in this regard, can be considered as a key energy carrier since it provides a high energy density per unit of mass and is completely carbon neutral at the use-point. For these reasons, the demand of hydrogen and of hydrogen-related products (i.e. e-fuels) for distributed uses is significantly rising [3]. A not-exhaustive list of possible uses includes H_2 for transportation (vehicles, trains) and for heat and power generation (fuel cells, CHP based systems) [4,5]. In this scenario, the use of hydrogen provides a significant option to reduce the CO_2 emissions [6] or completely decarbonize combustion-based processes at the stack. Despite the growing attention to the development of completely clean technologies, like electrolyzers, unbalances in the demand/generation curve and the lack of suitable transportation vectors hinder the large-scale application [7].

An alternative approach to facilitate the advancement of a hydrogen H_2-based network involves downsizing catalytic processes typically carried out on a large scale. This downsizing would make them more suitable for meeting the actual demand for hydrogen while also promoting H_2 utilization technologies. Among the various options available, the most commonly adopted one is the utilization of steam methane reforming (SMR), which serves as a reference catalytic process for H_2 production. Notable progress in the development of small-scale methane reformers was achieved by Kolb and co-workers [8].

These small-scale methane reformers offer intriguing possibilities, particularly in their ability to employ biogas as an alternative feedstock. By utilizing biogas, the production of hydrogen can be achieved in a manner that is free from fossil carbon, thereby promoting a cleaner and more sustainable hydrogen production process. Additionally, the feedstock required for these systems is also produced using small-scale plants, aligning with the current H_2 generation scenario and further enhancing its viability.

With respect to large scale applications, heat transfer strongly limits the productivity of small-scale reformers. The convective heat transfer mechanism in tubular packed bed reactors adopted for large-scale SMR reactors is promoted by high flow velocities since no thermal continuity exists between the catalyst pellets and between pellets and the reactor inner wall. Since small scale units with shorter tubes need to operate at much smaller flow velocities, convective heat transfer is hindered. Several solutions have been studied in the past decade to be able to operate small scale tubular reactors for nonadiabatic applications.

Microchannel reactors have been proposed for non-adiabatic reactions [9] thanks to their enhanced heat exchange areas and reduced thermal pathways. The concept is based on the close coupling of the domain where the reaction takes place and of the heat generation/removal region. A channel where catalytic combustion occurs is placed adjacent to a channel where the endothermic reforming reaction takes place. These systems are also characterized by very high surface areas that further promote the heat transfer between the two domains. The thermal conductivity of the reactor in this case is not vital, thanks to the intimate contact between the regions for heat release and heat consumption. Recently, a new kind of structured catalyst has been reported for the intensification of methane steam reforming at the small-scale thanks to the promotion of convective heat transfer by means of flow-guiding elements. Significant advantages in terms of overall heat transfer and hydrogen productivity at the same pressure drop of a conventional unit have been claimed [10].

Another approach, proposed first by Tronconi and Groppi [11], is the adoption of conductive reactor internals for intensifying heat transfer in both exothermic and endothermic applications. The change of the dominant heat transfer mechanism from convection to conduction allows to debottleneck radial heat transfer in small-scale reactors [12,13]. Several kinds of structured supports, characterized by high thermal conductivity have been proposed, including monoliths [14], sintered fibers, open-cell foams [15], 3D printed structures [16] and structured packings. Activation of these structures can be performed by conventional washcoating [17] (i.e. coating the whole surface of the structure with a thin layer of catalyst) or by packing them with small catalytic particles. The novel packed foam reactor, and the analysis of its heat transfer performances have been first described in the work of Visconti et al. [18]. The use of packed foams appears here as a suitable alternative to conductive monoliths, because it enables a higher catalyst inventory and a higher flow uniformity due to radial mixing. The application of foams to the intensification of the methane steam reforming process was first presented by Balzarotti et al. [19], in a work presenting a comparison between washcoated and packed foam configurations. According to the outcomes of this work the presence of the foam enables to strongly decrease the temperature gradient, and both washcoated and packed configurations are suitable for the intensification. In a later study [20] Balzarotti and co-workers investigated extensively the packed foam configuration, considering foams made of different materials (FeCrAlloy, Cu) and pore densities (Cu10, Cu40). The performance of the different internals was assessed quantitatively, by computing a global heat transfer coefficient by means of a new heat transfer model. The results proved the superior heat transfer performances of packed copper foam with high pore density (Cu40). One-to-one comparison with a packed bed reactor operated at the same external wall temperature, space velocity and catalyst loading demonstrated that at high temperature (equilibrium-controlled regime) the

system displays much lower temperature gradients for similar or higher methane conversion. An apparent advantage is also present at lower temperatures (kinetic controlled regime), since the system can operate at higher and more uniform temperatures, showing an increase in methane conversion up to 15%.

With the aim of predicting the packed foams behaviour, additional studies have been performed to describe the packed foams porosity and pressure drop [21] as a function of the cell diameter, the pore diameter and the pellet size.

This new contribution extends the previous work of Balzarotti [20] since the best performing system (Cu40) is tested under more intensified conditions (higher catalyst density and load) and up to 6 times higher volumetric flow rates to fully explore the potential of the technology. A slightly different design of the rig allowed to collect more controlled temperature profiles, showing that the presence of the packed foam enhances the radial heat transfer of a packed bed. However, a resistive gap is still present between the tube wall and the foam monolith. For the first time a more advanced 2D mathematical model is provided, which is essential to catch the real temperature distribution across the catalytic bed and allow for proper reactor design. An original pseudo-heterogeneous approach (one phase for mass balances, two phases for energy balances) is herein presented and is validated against the experimental data. Finally, the developed model is used to design a compact SMR unit (1 m length and 10 cm in diameter), that, despite its reduced dimension, is able to operate at industrial scale heat duties.

2. Experimental methods

In this work, the same Rh/Al_2O_3 catalyst described and characterized by Ambrosetti et al., 2022 [22] has been used. The egg-shell catalyst was prepared starting from alumina particles (Puralox by Sasol, 600 μm nominal diameter, d50 = 660 μm) that were preliminary dried in a static oven at 120 °C overnight and stabilized by a thermal treatment at 750 °C for 12 h. The pellets were activated by wet impregnation with an aqueous solution of $Rh(NO_3)_3$ (12.5%wt. metal content by Alfa Aesar). The amount of the solution was calculated with an excess of 25% with respect to the pellet pore volume, while the solution concentration was calibrated to reach a Rh content per mass of pellet equal to 0.3% wt. The thickness of the egg-shell, measured by optical microscope, was 38 $\pm$2μm; thus the composition of the catalytic layer is 1% wt. Rh/Al_2O_3.

Steam reforming tests were performed in a lab-scale rig, where methane is delivered by a Brooks 5851 mass flow controller, and liquid water is delivered by a Brooks IP40 QUANTIM and evaporated by a Brooks VDM300; after the evaporator, gas lines are electrically traced to prevent water condensation.

The reactor is externally heated by a three-zone electric furnace (Carbolite Gero, EVZ 1200), whose temperature control is independent from the reactor temperature measurement. The reactor was heated by setting the oven temperature. The reactor is a stainless-steel tube (AISI 310 S), 68 cm long and with internal and external diameter of 2.95 cm and 3.4 cm, respectively. It is equipped with three stainless steel thermowells with sliding Type-K thermocouples: one is positioned at the centerline of the reactor, the second one is located at mid-radius, whereas the third thermowell is welded on the external surface of the tube wall. The temperature profiles of the reactor were measured with a spatial resolution of 0.5 cm.

Downstream from the reactor, the product stream is cooled in a glycol-cooled shell and tube condenser to remove water. Dry gases are recovered from the top of the condenser and fed to an additional water trap before being sent to the analyzer. Prior to sampling, the dry products are mixed with a controlled N_2 flow (about 1/3 of the inlet methane flow) acting as internal standard; analysis is performed by a Pollution GCX micro-gas chromatograph equipped with MolSieve and Porapack columns connected to TCD detectors for online quantification.

Concentrated methane/steam feeds were tested in this work with fixed steam-to-carbon, equal to 4.1. The start-up procedure of the system consisted of pre-heating the bed in N_2 up to a temperature of 500 °C, after which steam was fed to the reactor. The system was then left in steam/N_2 mixture for half an hour; afterwards methane was fed in the reactor while removing N_2 and the oven temperature was heated to the desired set-point value. An inverse procedure was adopted for the shut-down: the methane feed was first replaced with N_2 and the system was cooled down to 500 °C in N_2/water, then water feed was stopped and the system was cooled down at room temperature in inert flow.

Reactor internals (foam configuration and catalyst inventory) and operating conditions were selected to test the packed-foam configuration under highly intensified heat demand, if compared to our previous work [20]; at this scope, bed dilution was drastically reduced, and space velocities were significantly increased. Copper foams were selected based on the results of Balzarotti et al., 2020 [20]: ERG Duocell (cell diameter d_{cell}=2 mm, void fraction ε_f=0.88) were chosen as best performing foams. Foams disks with a thickness of 1.25 cm, an external diameter of 2.95 cm with additional holes to place the thermowell were cut from panes provided by ERG Aerospace (the holes were obtained with the waterjet technique, allowing for precise samples with ±0.1 mm error). The catalytic bed consisted of a stack of 5 copper foams with 5.08 g of inert pellets and 21.92 g of Rh/Al_2O_3 catalyst. On top of the catalytic bed, one additional foam was added and packed with inert alumina pellets. Fig. 1a shows a picture taken during the reactor loading procedure, where the 6 copper foams can be recognized. Fig. 1b shows the complete scheme of the reactor, in which the gases flow from the top downwards: once entering the reactor, the gases encountered first a bed of 3 cm of inert Al_2O_3 pellet (d_{pellet}=1.6 mm Puralox by Sasol), a spacer consisting of a 2 mm thick disc of high PPI Cu-foam (Alantum), and a bare foam. This section guarantees homogeneous mixing and heating on the feed stream that enters into the catalytic bed. Another bare copper foam is placed downstream from the catalytic bed, followed by a FeCrAlloy foam, that is placed atop of a disk solidly welded to the thermowells of the system that was also able to keep the catalytic bed in the isothermal zone of the reactor.

Table 1 summarizes for each experimental test, the particle Reynolds number (Re_{dp}), the oven temperature and the gas hourly space velocity (GHSV). Space velocities are referred both to the catalyst mass and to the reactor volume: the former is more suitable for kinetic considerations, whereas the latter is more useful for scale-up evaluations. The reference volume considered is the portion of reactor including the foams packed with the Rh-based catalyst. It can be observed that the calculated Re_{dp} are much smaller than the typical industrial ones, where larger particles and higher gas velocities are used to cope with the trade-off of acceptable pressure drop and sufficiently high convective heat transfer. Such a trade-off completely changes with the new configuration of the packed foam reactor, where convection and radial heat transfer mechanisms are independent.

All the tests were performed with a steam to carbon ratio, S/C= 4.1. During the campaign, no experimental evidence of coke formation or catalyst activity loss was collected. This is in agreement with the outcomes of a previous work, where the catalyst went through more severe conditions (lower S/C) [22].

3. Mathematical model

A 2D heterogeneous model of the steam reforming reactor was developed starting from the knowledge previously gained on heat transfer mechanisms in packed foams [20,23].

The model consists of two separate energy balances for the solid foam and a pseudo-phase, which lumps the catalyst particles and the gas flowing phase. These latter are assumed to be at the same temperature given the very large specific surface areas of the pellets and the relatively high Nu numbers.

Mass balances, for H_2O, CH_4, CO, CO_2, H_2 in the pseudo-phase, are considered, keeping the assumption of negligible mass transfer resistance between the gas and the catalyst particles.

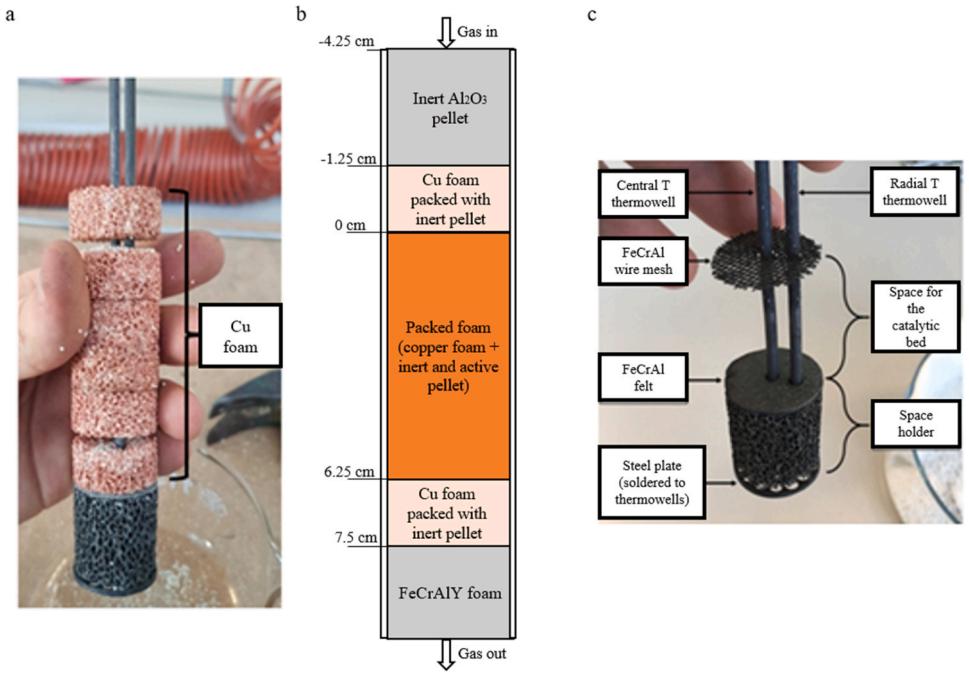

Fig. 1. (a) Pictures of the catalytic bed during the reactor loading procedure, (b) reactor layout and (c) system assemblage.

Table 1
Operating conditions used for testing the tubular lab-scale reactor.

Test number	Re_{dp}	GHSV $\left[\frac{Nm^3}{kg_{cat}\cdot h}\right]$	Oven temperature [°C]
1	1.8	10	750
2			700
3			650
4			600
5	2.7	15	800
6			750
7			700
8	3.5	20	800
9			750
10			700
11	5.3	30	800

i-species mass balance

$$G\cdot\frac{\partial\omega_i}{\partial z}=\rho_{mix}\frac{\partial}{\partial z}\left(D_{(eff,z)i}\cdot\frac{\partial\omega_i}{\partial z}\right)+\rho_{mix}\frac{1}{r}\frac{\partial}{\partial r}\left(D_{(eff,r)i}\cdot r\cdot\frac{\partial\omega_i}{\partial r}\right)+\sum_{j=1}^{Nreac}\nu_{ij}\cdot r_j\cdot\eta_j\cdot MW_i\cdot CI \quad (1)$$

Where:

- G is the total specific mass flow rate in [kg/m^2/s];
- ω_i is the mass fraction of the species i;
- ρ_{mix} is the density of the gaseous mixture in [kg/m^3];
- $D_{(eff,z)i}$ and $D_{(eff,r)i}$ are the effective axial and radial diffusion coefficient in [m^2/s], computed according to Delgado, 2007 [24];
- r_j are the rates of j - reaction in [mol/g$_{cat}$/s] calculated according to the kinetic model of Ambrosetti et al., 2021 [22] (Supplementary Information, Section S4). In addition, the internal mass transfer limitations are taken into account using a Thiele modulus approach assuming pseudo 1st order kinetics in the limiting reactant;
- MW_i is the molar weight of the species i in [kg/mol];

The energy balance on the metallic foam is

$$\frac{\partial}{\partial z}\left(k_{f,z}\cdot\frac{\partial T_f}{\partial z}\right)+\frac{1}{r}\frac{\partial}{\partial r}\left(k_{f,r}\cdot r\cdot\frac{\partial T_f}{\partial r}\right)=h_{pf}\cdot S_v\cdot\left(T_f-T_p\right) \quad (2)$$

Concerning the pseudo-phase, the energy balance is the sum of the energy balance on the gas phase and of the energy balance on the pellets

$$G\cdot cp_{mix}\cdot\frac{\partial T_p}{\partial z}=\frac{\partial}{\partial z}\left(k_{p,z}\cdot\frac{\partial T_p}{\partial z}\right)+\frac{1}{r}\frac{\partial}{\partial r}\left(k_{p,r}\cdot r\cdot\frac{\partial T_p}{\partial r}\right)+h_{pf}\cdot S_v\cdot\left(T_f-T_p\right)+\sum_{j=1}^{n^\circ reactions}r_j\cdot CI\cdot\Delta H_{reaz,j} \quad (3)$$

with

- T_f and T_p as the temperatures of the foam and of the pseudo-phase in [K];

- $k_{p,z}$ and $k_{p,r}$ [W/m/K] are the axial and radial effective conductivities for the pseudo-phase, calculated with the correlation of Specchia et al. 1980 [25], whereas $k_{f,z}$ and $k_{f,r}$ [W/m/K] are the effective axial and radial thermal conductivities of the foam, which depends on foam porosity and bulk conductivity of the metal according to the correlation of Bracconi et al., 2018 [26];
- The interphase heat transfer coefficient h_{pf} [W/m^2/K] is computed with the correlation of Specchia et al. 1980 [25] considering an equivalent tube diameter equal to the foam cell size and filled with catalyst pellets;
- S_v is the specific surface area in [1/m];
- $\Delta H_{reaz,j}$ is the enthalpy of reaction j in [J/mol].

Details on calculations of effective conductivities and heat transfer coefficients are reported in Supplementary Information, Section S5.

In order to account for pressure drop, 1D Ergun equation [27] was used considering the average flow properties in radial direction

$$\frac{\partial P}{\partial z}=-\left(4.17\cdot\frac{S_{v,tot}^2}{\varepsilon_{tot}^3}\cdot\overline{\mu}_{mix}\cdot\overline{v}+0.292\cdot\frac{S_{v,tot}}{\varepsilon_{tot}^3}\cdot\overline{\rho}_{mix}\cdot\overline{v}^2\right) \quad (4)$$

with $\overline{\mu}_{mix}$ and $\overline{v}$ as the average gas viscosity and velocity. The Ergun

equation is corrected by the overall void fraction (ε_{tot}) and by the total surface which is in contact with the gas ($S_{v,tot}$). Here

- The total wetted surface $S_{v,tot}$ in [1/m] is given by the sum of the foam surface ($S_{v,foam} = 1220m^{-1}$) and of the pellet surface ($S_{v,pellet} = 3030m^{-1}$). The first one is inversely proportional to the cell diameter [21,28], the second one depends on the pellet diameter and on the porosity of the packing pattern.
- The total void fraction ε_{tot} is given by the product of the foam void fraction (ε_{foam}) and of the packed bed void fraction ($\varepsilon_{packedbed}$)
- The flow viscosity, velocity and density are respectively $\overline{\mu}_{mix}$, $\overline{v}$ and $\overline{\rho}_{mix}$

The boundary conditions of the momentum balance consist in imposed outlet pressure at the outlet and the boundary conditions for mass and energy balances are reported in Table 2.

At the reactor inlet, Danckwerts boundary conditions were considered for the mass balances. Concerning the pseudo-phase energy balance, the temperature was set equal to the inlet experimental one and a null axial derivative was set for the foam temperature. At the reactor outlet a null derivative was considered for all mass fractions and temperatures. Along the axis, null radial derivatives were considered as a symmetry condition for mass fractions and temperatures. At the reactor wall, null radial derivatives were imposed to mass fractions (impermeable wall) whereas a heat flux continuity was imposed for both phases, by means of wall heat transfer coefficients calculated according to Specchia et al., 1980 [25] for the pseudo-phase and Aghaei et al. [29] for the solid foam. A wall temperature profile T_W was imposed, calculated by interpolation of measured T points.

The model was implemented in Matlab. Axial derivatives were discretized with backwards finite differences and radial derivatives were discretized with symmetric orthogonal collocations. 61 axial points and 7 radial collocation points were considered for the numerical solution. The resulting set of algebraic equations was solved in Matlab with the numerical routine fsolve with sparse Jacobian matrix.

4. Experimental results

4.1. Conversion performances

Methane steam reforming tests were performed at different GHSV and oven temperatures. In Fig. 2 are reported the experimental CH_4 conversion (panel 2a) and the ratio $(\mathrm{RadialT_{OUT}} - \mathrm{RadialT_{IN}})/(\mathrm{T_{fur}} - \mathrm{RadialT_{IN}})$ (panel 2b) is a function of GHSV for different oven temperatures. As expected, CH_4 conversion increases on increasing the oven temperature and on decreasing the GHSV. The ratio is closer to one the lower GHSV is, due to the lower energy demand of the inlet flow. Plotting the conversion data point vs the measured outlet temperatures at mid radius (panel 2c), which is a reasonable proxy of the average temperature across the reactor cross section as already reported in our previous work by Balzarotti et al., 2020 [20], clearly shows that the system was able to achieve equilibrium conditions under all the investigated conditions, indicating that conversion performances are controlled by the heat transfer rate and are not limited by kinetics.

In Fig. 3, the outlet molar fractions are plotted against the outlet temperature at mid radius. Comparison with the corresponding equilibrium values confirms that under the explored operating conditions the reactor works under thermal control.

A small deviation from equilibrium is observed when the outlet temperature decreases after lowering the furnace set point temperature or increasing the flow rate.

Notably, we were able to operate the steam reforming reaction in a lab-scale configuration approaching the thermodynamic limit with specific power duties in the range of 2–9 MW/m^3, corresponding to average heat fluxes of 15–70 kW/m^2 referred to the outer surface of the reaction tube (see Supplementary Information, Section S1 and S2 for calculation details). Such values are comparable with those of industrial tubular reformer [10].

Table 2
Boundary conditions.

Domain	Mass balances	Pseudo-phase energy balance	Foam energy balance
$z = 0;\quad 0 \le r \le R_o$	$D_{(eff,z)_i} \cdot \frac{\partial \omega_i}{\partial z} = v_{in} \cdot (\omega_i - \omega_{i,0-})$	$T_p - T_{p0^+}(r) = 0$	$\frac{\partial T_f}{\partial z} = 0$
$z = L;\quad 0 \le r \le R_o$	$\frac{\partial \omega_i}{\partial z} = 0$	$\frac{\partial T_p}{\partial z} = 0$	$\frac{\partial T_f}{\partial z} = 0$
$0 < z < L;\quad r = 0$	$\frac{\partial \omega_i}{\partial r} = 0$	$k_{p,r} \cdot \frac{\partial T_p}{\partial r} = 0$	$k_{f,r} \cdot \frac{\partial T_f}{\partial r} = 0$
$0 < z < L;\quad r = R_o$	$\frac{\partial \omega_i}{\partial r} = 0$	$k_{p,r} \cdot \frac{\partial T_p}{\partial r} = h_w \cdot (T_W - T_p)$	$k_{f,r} \cdot \frac{\partial T_f}{\partial r} = h_{wf} \cdot (T_W - T_f)$

4.2. Axial temperature profiles

To gain insight in the thermal behavior of the reactor, axial temperature profiles were collected along the axis (Central T), at mid-radius position (Radial T) and along the outer wall of the reaction tube (Wall T). In Fig. 4, typical axial temperature profiles are plotted to discuss some common features observed in steam reforming tests. Here, the temperature profiles are considered from the beginning of the upper foam packed with inert pellets, to the end of the foam packed with catalytic pellets. In the figures, these two zones are delimited by a dashed vertical line.

Gas enters the rector at 610 °C, i.e., well below the wall temperature. A marked difference between the wall temperature and the furnace set point is evident in the whole bed, consistent with the very high heat fluxes imposed in the test. Looking at the mid-radius and centerline temperature profiles, a drop of the temperature is evident already before the entrance of the catalytic bed, due to heat back-diffusion. The cold-spot is located a few millimeters after the entrance of the bed, after which the temperature grows reducing progressively the difference from the wall temperature, as expected in systems controlled by heat transport. Despite the extreme conditions, however, radial temperature differences between the two thermocouples inserted in the bed are quite small and are much lower than the difference between the mid-radius and the vall temperatures.

This behavior is in line with previous findings of our group that identify the wall heat transfer as the controlling heat transfer resistance in these systems. In fact, the internal temperature profiles are flattened thanks to the very high radial thermal conductivity ensured by the copper foams.

Fig. 5 compares the temperature profiles collected at the same oven temperature and different GHSV.

By considering the temperature profiles we can notice that, on increasing GHSV:

- The distance between the furnace set temperature and the wall temperature increases, due to the higher heat demand.
- The inlet temperature decreases due to a reduced pre-heating efficiency across the inert zone upstream from the catalyst.
- The extent of the cold-spot grows and its position moves towards the outlet of the reactor. However, in all cases the cold spot occurs well within the first half of the bed. We ascribe this behaviour both to the reduction of the contact time and to the reduction of the temperature in the bed that slows the reaction kinetics. Internal radial temperature gradients independent of the space velocity and the two internal temperature profiles are almost superimposed. This is consistent with the conductive internal heat transfer mechanism secured by the copper foam, in contrast with what is typically observed for packed bed reactors (see Balzarotti et al. 2020 [20]).

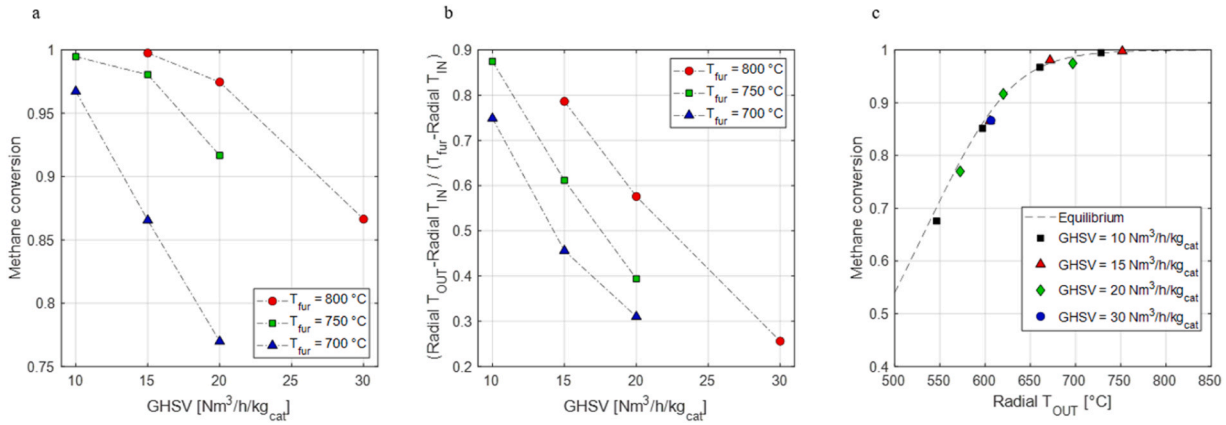

Fig. 2. (a) Outlet methane conversion for different oven temperatures and GHSV; (b) ratio between outlet temperature in mid-radius position and the oven temperature, for different GHSV; (c) Experimental methane conversion against thermal equilibrium.

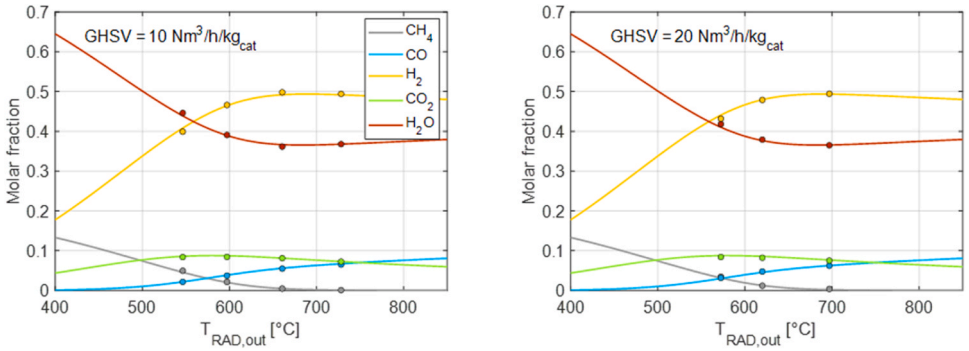

Fig. 3. Outlet molar fractions (symbols) and thermodynamic equilibrium (curves).

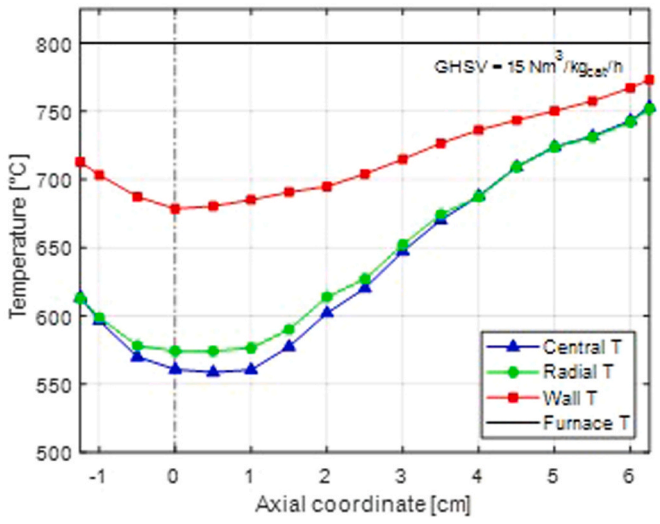

Fig. 4. Experimental temperature profiles for Test 5: GHSV 15 $Nm^3/kg_{cat}/h$ and furnace temperature 800 °C. The vertical dotted line delimits the foam packed with inert pellets from the foam packed with catalytic pellet.

- In the second part of the reactor, the internal temperature profiles gradually approach the wall temperature. However, only at the lowest space velocities the set-point temperature is closely approached.

Fig. 6 presents three temperature profiles obtained for different furnace temperatures, at fixed GHSV of 15 $Nm^3/kg_{cat}/h$. It is possible to observe that:

- The extent of the cold-spot is a function of the reaction temperature since at lower temperature the process kinetics are slower, which leads also to a progressive shift of the cold-spot towards the end of the bed by reducing the temperature of the system.
- In the case of high temperature tests, the slope of the profile after the cold-spot is much higher than in the case of low-temperature tests.

5. Simulations results

The 2D model presented in Section 3 was used to predictively simulate the experimental data. In particular, the temperature and composition profiles of the area between the beginning of the foam packed with inert and the end of the foam packed with the catalytic pellet were simulated. This was achieved by solving the system of equations considering null reaction rates before entering the catalytic bed.

A preliminary comparison between model results and experiments was performed by comparing the methane conversions. The parity plot in Fig. 7. shows a 5% maximum deviation of the model from the experiments, which confirms the reliability of the numerical simulations.

The accuracy of the model in describing the thermal behavior of the packed foam reactor is more stringently verified by the analysis of the temperature profiles. Fig. 8 compares the measured temperature profiles with the simulated solid temperatures at the centerline and the mid-radius positions (dashed lines) and with the pseudo-phase temperature (solid lines). The model is able to quantitatively describe the temperature profiles in the system, well capturing the proximity of the internal profiles as well as the difference of the internal profile from the wall temperature, confirming the adequacy of the implemented heat

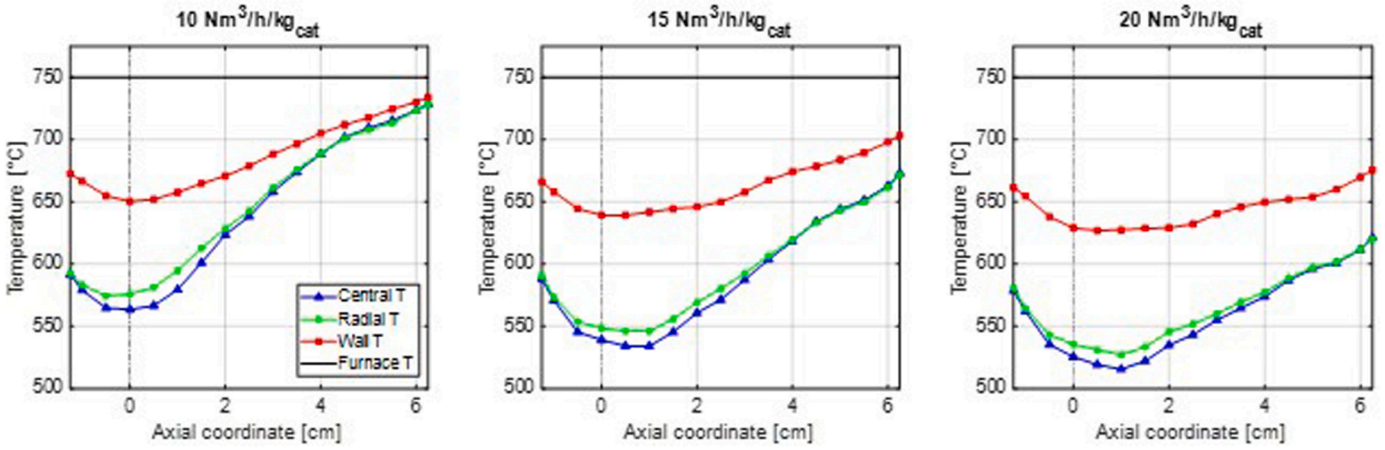

Fig. 5. Measured temperature profiles at varying GHSV and same furnace temperature (750 °C).

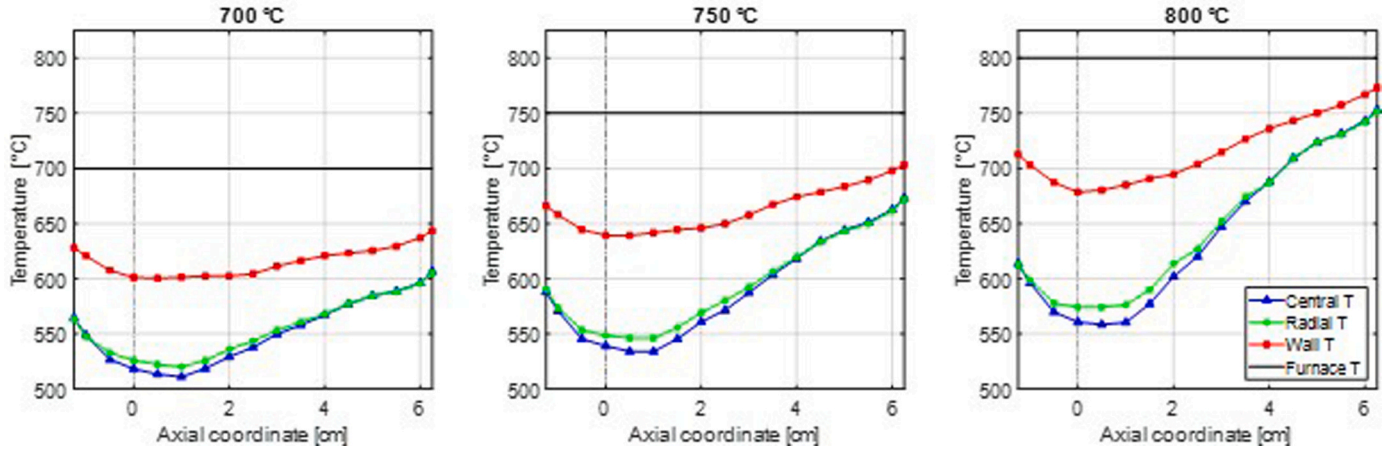

Fig. 6. Measured temperature profiles at increasing furnace temperature (700, 750, 800 °C) at GHSV = 15 $Nm^3/kg_{cat}/h$.

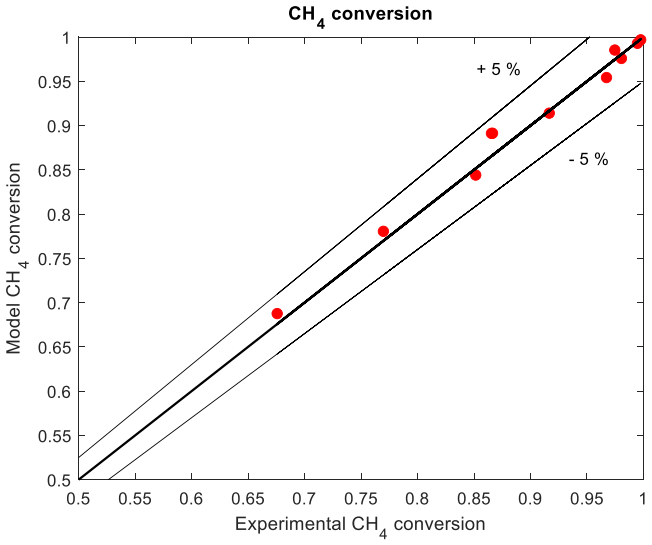

Fig. 7. Parity plot comparing predicted and experimental methane conversions.

transport model. It can be observed that the model can well predict the inlet temperature of the catalytic zone. However, a systematic deviation in the inlet region is evident, since the simulated cold spot is closer to the reactor inlet with a minimum temperature 10–15 °C higher. This can be explained by heat back diffusion in the thermowell that can mitigate the extent of the cold spot. Other small discrepancies in the temperature estimates can be found at the very end of the reactor. This small difference can be due to the null derivatives imposed as boundary conditions, implying no heat exchange at the end of the packed foam, whereas the real system continues to exchange heat with the oven and with a conductive foam. The control of heat transfer is however dominated by the values by the heat transfer coefficients at the wall for the two phases h_w and h_{wf} (a sensitivity analysis in SI, Section S7). The deviations from the experimental profiles are however in a narrow temperature range (5–10 °C), therefore we conclude that the model can successfully predict the outlet temperature and the shape of the temperature profile without adjusting any adaptive parameter. Additional model results, in particular for the simulation of composition profiles along the reactor axis, can be found in SI, Section 3.

6. Case study: 30 Nm^3/h compact packed foam reformer

The model was used for a preliminary design of a scaled-up unit, which is suitable for integration into a compact power generation system for residential applications [5]. The aim of this study is to prove that the packed-foam concept can be successfully implemented by adjusting a few design parameters.

Operative conditions of the reactor were slightly changed to meet semi-industrial requirements. In particular, the outlet pressure was set to 7 bar, a pressure level that allows a proper design of a PSA for hydrogen

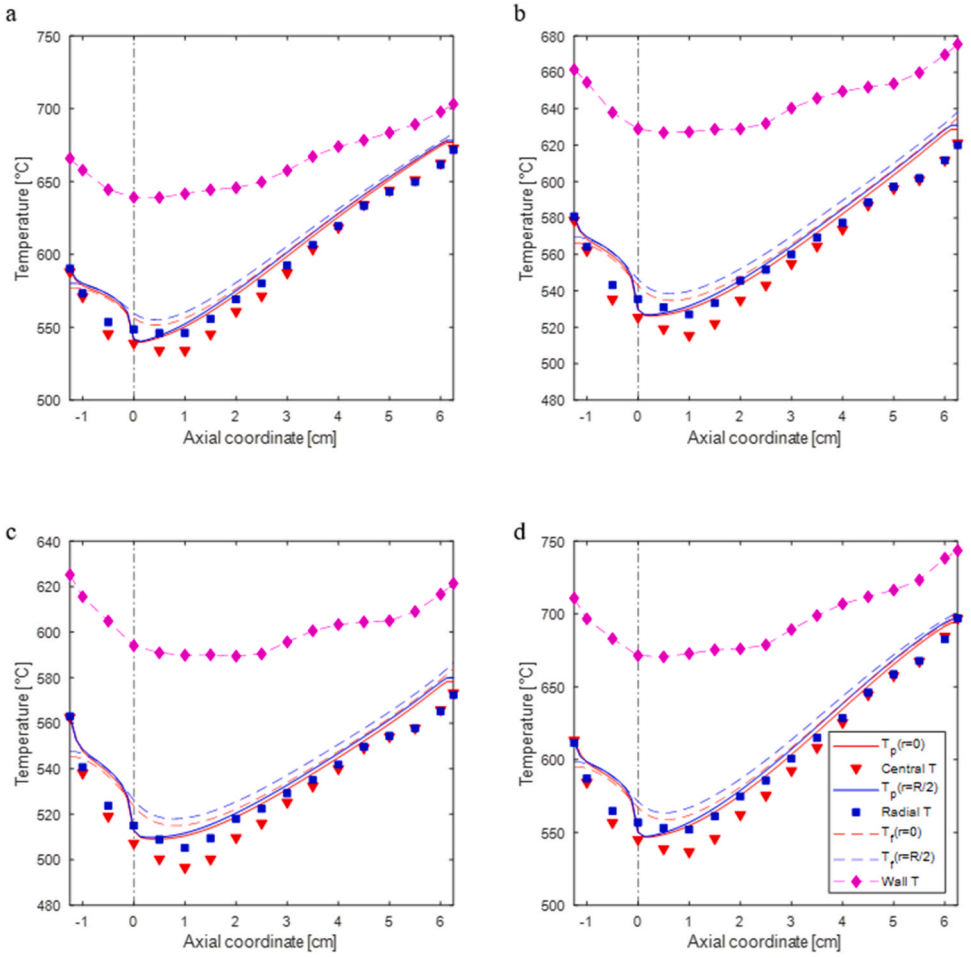

Fig. 8. Temperature profiles along the reactor length: comparison between experimental and simulated results for different operating conditions: (a) T_{fur} 750 °C, 15 $Nm^3/h/kg_{cat}$, (b) T_{fur} 750 °C, 20 $Nm^3/h/kg_{cat}$, (c) T_{fur} 700 °C, 20 $Nm^3/h/kg_{cat}$, (d) T_{fur} 800 °C, 20 $Nm^3/h/kg_{cat}$.

separation. A uniform wall temperature was assumed equal to 850 °C, taken as a safe condition for reactor tube walls, copper internals and Rh-based catalyst.

The same Cu foam microgeometry and catalyst pellets size and activity adopted in the experimental part of the work were considered here, whereas the reactor length, diameter and GHSV were set based on some process constraints (e.g. ensuring an outlet methane conversion higher than 90% and pressure drop lower than 1 bar/m).

The case study considered a unit operating at GHSV = 10 [$Nm^3/kg_{cat}/h$] where the Cu foam has the same properties as the experimentally tested internals, being 1 m long and 10 cm wide. An inlet temperature of 550 °C was considered, similarly to the one observed in the experiments. To approach industrial conditions, a steam to carbon ratio of 3.5 was adopted, which is lower than in laboratory tests.

Considering undiluted catalyst packing, with void fraction of 0.5 (as discussed for pellets with diameter dp = 0.66 mm inside a copper foam with d_{cell} = 2 mm and dpore = 1 mm is by Ambrosetti et al., 2020 [21]), a catalyst mass of 4.1 kg was assumed: for the treated GHSV value, this entails a methane feed flow rate of 9 [Nm^3/h].

For the selected operating conditions, from the simulation results, the methane conversion is 93% and the hydrogen productivity is of 29.4 [Nm^3/h] with an acceptable pressure drop of approximately 0.6 bar.

Fig. 9 displays the axial profiles of the calculated mole fractions inside the reactor, together with the compositions at equilibrium. Thermodynamic equilibrium of the system is reached a few centimetres after the inlet, also due to the mid pressure which speeds up the quasi first order reforming kinetics (Supplementary Information, Section S4),

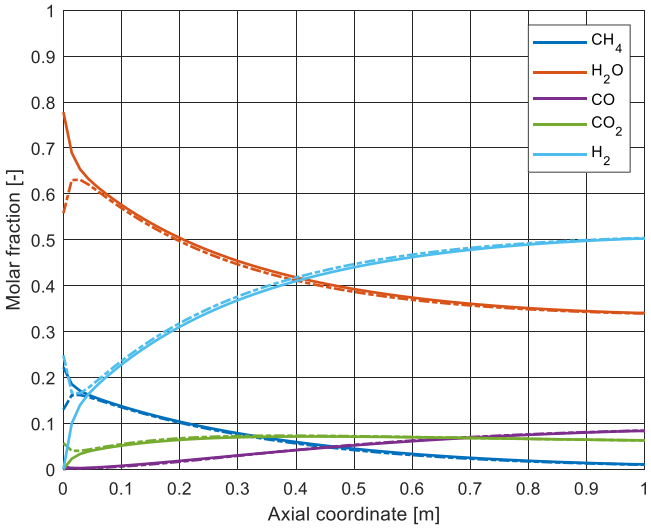

Fig. 9. Simulated molar fraction profiles along the reactor length (solid lines) and equilibrium molar fractions (dotted lines) for the case study of scaled-up intensified packed-foam reactor.

proving that the system is under full thermal control.

Fig. 10 shows axial temperature profiles, at different radial coordinates, for the pseudo-phase (gas and pellet) and foam. A rather

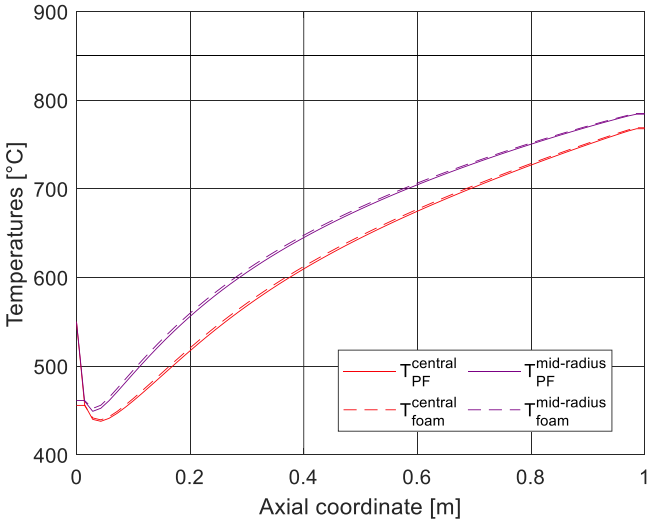

Fig. 10. Simulated temperature profiles along the reactor length for the pseudo-phase (solid lines) and solid phase (dotted lines), the solid black line represents the constant wall temperature.

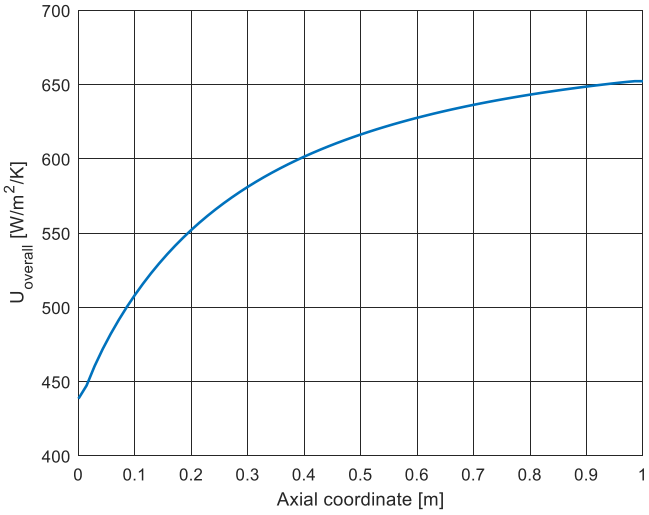

Fig. 11. Overall heat exchange coefficient profile.

pronounced cold spot occurs a few centimetres from the reactor inlet. Downstream, similarly to the lab-scale tests, the temperature rises towards the reactor outlet up to almost 800 °C.

Calculated temperature profiles show that, despite the large diameter, the internal profiles keep close (less that 25 °C difference) all along the bed, whereas the wall temperature is always much higher than the internal ones, indicating that the limiting heat transfer resistance is still the one at the interface between the tube wall and the packed foam. It can be observed that very limited temperature differences between the phases are present, due to the very high surface area of the adopted foam.

Using the temperature and cupmix gas compositions, it was possible to estimate a global heat exchange coefficient (Balzarotti et al., 2020 [20], more details can be found in SI, Sections 5 and 6). Results are reported in Fig. 11 showing that $U_{overall}$ values ranging from 450 W/m^2/K to 650 W/m^2/K are calculated along the catalyst bed, the increasing trend being mainly associated to the high thermal conductivity of H_2, which is progressively produced through the bed. The high heat transfer coefficients allow to achieve a specific power duty of 3.6 MW/m^3 with an average heat flux of 90 kW/m^2.

These results prove that the use of packed foams makes possible to achieve at small scale heat transfer performances comparable with larger industrial plants, paving the way for the intensification of steam reforming of methane for more distributed, small-scale hydrogen production.

7. Conclusions

The development of small-scale reactors with enhanced heat transfer properties has key importance in advancing efficient processes, particularly in the context of hydrogen production. Overcoming technological challenges is crucial to ensure the efficient distribution and utilization of hydrogen. In this study, experimental testing and mathematical modelling of an intensified methane steam reforming reactor are presented, utilizing copper open-cell foams packed with a highly active Rh catalyst.

Starting from a preliminary work of our group [20], an extended experimental campaign focused on achieving a high degree of intensification for small-scale methane reformers was performed. This effort resulted in promising hydrogen productivity and heat transfer performance. Despite the demanding conditions, the inclusion of conductive internals enabled to operate the reactor close to thermodynamic equilibrium, achieving methane conversions exceeding 90%.

Mathematical modelling of this reactor concept was addressed by developing an original hybrid heterogeneous 2D mathematical model of nonadiabatic packed foam reactors. This model successfully predicts inter-phase and radial temperature gradients, which are well aligned with the experimental data. These encouraging results create a basis for utilizing the 2D model in reactor design, enabling the prediction of performance for reactors with internal conductive structures of different geometries (e.g., packed POCS). Furthermore, this model can be extended to other heat-transfer limited processes where accurate estimation of radial temperature profiles is crucial, such as Fischer-Tropsch synthesis. The model was then applied for the design of a tentative unit for small scale applications. We demonstrate the feasibility of small-scale reformers (1 m long) with comparable hydrogen productivities as large-scale plants thanks to the improved heat transfer performances.

CRediT authorship contribution statement

Giulia Ferri: Conceptualization, Data curation, Methodology, Investigation, Software, Validation, Formal analysis, Visualization, Writing – original draft. **Matteo Ambrosetti:** Conceptualization, Methodology, Investigation, Software, Validation, Supervision, Resources, Writing – review & editing, Project administration. **Alessandra Beretta:** Conceptualization, Methodology, Supervision, Resources, Writing – review & editing, Project administration. **Gianpiero Groppi:** Conceptualization, Methodology, Supervision, Resources, Writing – review & editing, Project administration. **Enrico Tronconi:** Conceptualization, Methodology, Supervision, Resources, Writing – review & editing, Project administration, Funding acquisition.

Declaration of Competing Interest

The authors declare that they have no known competing financial interests or personal relationships that could have appeared to influence the work reported in this paper.

Data Availability

Data will be made available on request.

Acknowledgements

This project has received funding from the European Research Council (ERC) under the European Union's Horizon 2020 research and

innovation programme (GA No 966725) and (GA No. 694910).

Appendix A. Supporting information

Supplementary data associated with this article can be found in the online version at doi:10.1016/j.cattod.2023.114386.

References

[1] L. Baharudin, M. James Watson, Hydrogen applications and research activities in its production routes through catalytic hydrocarbon conversion, Rev. Chem. Eng. 34 (2017) 43–72, https://doi.org/10.1515/revce-2016-0040.

[2] J.R. Rostrup-Nielsen, Catalytic Steam Reforming, in: 1984: pp. 1–117. https://doi.org/10.1007/978–3-642–93247-2_1.

[3] J.M. Bermudez, S. Evangelopoulou, F. Pavan, Hydrogen Report, (2021). Available online at https://www.iea.org/reports/hydrogen (accessed August 29, 2023).

[4] S. Ahmed, Hydrogen from hydrocarbon fuels for fuel cells, Int J. Hydrog. Energy 26 (2001) 291–301, https://doi.org/10.1016/S0360-3199(00)00097-5.

[5] S. Specchia, Fuel processing activities at European level: a panoramic overview, Int J. Hydrog. Energy 39 (2014) 17953–17968, https://doi.org/10.1016/j.ijhydene.2014.04.040.

[6] M.A. Ashraf, S. Tacchino, N.R. Peela, G. Ercolino, K.K. Gill, D.G. Vlachos, S. Specchia, Experimental insights into the coupling of methane combustion and steam reforming in a catalytic plate reactor in transient mode, Ind. Eng. Chem. Res 60 (2021) 196–209, https://doi.org/10.1021/acs.iecr.0c04837.

[7] K.M. Van Geem, B.M. Weckhuysen, Toward an e-chemistree: materials for electrification of the chemical industry, MRS Bull. 46 (2021) 1187–1196, https://doi.org/10.1557/s43577-021-00247-5.

[8] R. Zapf, R. Thiele, M. Wichert, M. O'Connell, A. Ziogas, G. Kolb, Application of rhodium nanoparticles for steam reforming of propane in microchannels, Catal. Commun. 41 (2013) 140–145, https://doi.org/10.1016/j.catcom.2013.07.018.

[9] H. Yu, H. Chen, M. Pan, Y. Tang, K. Zeng, F. Peng, H. Wang, Effect of the metal foam materials on the performance of methanol steam micro-reformer for fuel cells, Appl. Catal. A Gen. 327 (2007) 106–113, https://doi.org/10.1016/j.apcata.2007.05.003.

[10] F. Minette, L.C. de Almeida, J. Feinstein, J. De Wilde, Structured ZoneFlow™-Bayonet steam reforming reactor for reduced firing and steam export: pressure drop and heat transfer modelling and evaluation of the reactor performance, Chem. Eng. J. Adv. 10 (2022), https://doi.org/10.1016/j.ceja.2022.100258.

[11] E. Tronconi, G. Groppi, T. Boger, A. Heibel, Monolithic catalysts with "high conductivity" honeycomb supports for gas/solid exothermic reactions: characterization of the heat-transfer properties, : Chem. Eng. Sci. (2004) 4941–4949, https://doi.org/10.1016/j.ces.2004.07.018.

[12] G.D. Wehinger, Improving the radial heat transport and heat distribution in catalytic gas-solid reactors, Chem. Eng. Process. - Process. Intensif. 177 (2022), 108996, https://doi.org/10.1016/j.cep.2022.108996.

[13] G.R. George, M. Bockelmann, L. Schmalhorst, D. Beton, A. Gerstle, A. Lindermeir, G.D. Wehinger, Optimization of metal foam pellet shape in packed beds for improved radial heat transfer using particle-resolved computational fluid dynamics, Chem. Eng. Process. - Process. Intensif. 188 (2023), https://doi.org/10.1016/j.cep.2023.109357.

[14] E. Tronconi, G. Groppi, C.G. Visconti, Structured catalysts for non-adiabatic applications, Curr. Opin. Chem. Eng. 5 (2014) 55–67, https://doi.org/10.1016/j.coche.2014.04.003.

[15] L. Fratalocchi, C.G. Visconti, G. Groppi, L. Lietti, E. Tronconi, Intensifying heat transfer in Fischer-Tropsch tubular reactors through the adoption of conductive packed foams, Chem. Eng. J. 349 (2018) 829–837, https://doi.org/10.1016/j.cej.2018.05.108.

[16] C.G. Visconti, M. Panzeri, G. Groppi, E. Tronconi, Heat transfer intensification in compact tubular reactors with cellular internals: a pilot-scale assessment of highly conductive packed-POCS with skin applied to the Fisher-Tropsh synthesis., 2023.

[17] M. Ambrosetti, R. Balzarotti, C. Cristiani, G. Groppi, E. Tronconi, The influence of the washcoat deposition process on high pore density open cell foams activation for CO catalytic combustion, Catalysts 8 (2018), https://doi.org/10.3390/catal8110510.

[18] C.G. Visconti, G. Groppi, E. Tronconi, Highly conductive "packed foams": a new concept for the intensification of strongly endo- and exo-thermic catalytic processes in compact tubular reactors, Catal. Today 273 (2016) 178–186, https://doi.org/10.1016/j.cattod.2016.02.060.

[19] R. Balzarotti, A. Beretta, G. Groppi, E. Tronconi, A comparison between washcoated and packed copper foams for the intensification of methane steam reforming, React. Chem. Eng. 4 (2019) 1387–1392, https://doi.org/10.1039/c9re00125e.

[20] R. Balzarotti, M. Ambrosetti, A. Beretta, G. Groppi, E. Tronconi, Investigation of packed conductive foams as a novel reactor configuration for methane steam reforming, Chem. Eng. J. 391 (2020), https://doi.org/10.1016/j.cej.2019.123494.

[21] M. Ambrosetti, M. Bracconi, M. Maestri, G. Groppi, E. Tronconi, Packed foams for the intensification of catalytic processes: assessment of packing efficiency and pressure drop using a combined experimental and numerical approach, Chem. Eng. J. 382 (2020), 122801, https://doi.org/10.1016/j.cej.2019.122801.

[22] M. Ambrosetti, D. Bonincontro, R. Balzarotti, A. Beretta, G. Groppi, E. Tronconi, H2 production by methane steam reforming over Rh/Al2O3 catalyst packed in Cu foams: a strategy for the kinetic investigation in concentrated conditions, Catal. Today 387 (2022) 107–118, https://doi.org/10.1016/j.cattod.2021.06.003.

[23] M. Ambrosetti, G. Groppi, W. Schwieger, E. Tronconi, H. Freund, Packed periodic open cellular structures – an option for the intensification of non-adiabatic catalytic processes, Chem. Eng. Process. - Process. Intensif. 155 (2020), 108057, https://doi.org/10.1016/j.cep.2020.108057.

[24] J.M.P.Q. Delgado, Longitudinal and transverse dispersion in porous media, Chem. Eng. Res. Des. 85 (2007) 1245–1252.

[25] V. Specchia, G. Baldi, S. Sicardi, Heat transfer in packed bed reactors with one phase flow, Chem. Eng. Commun. 4 (1980) 361–380, https://doi.org/10.1080/00986448008935916.

[26] M. Bracconi, M. Ambrosetti, M. Maestri, G. Groppi, E. Tronconi, A fundamental analysis of the influence of the geometrical properties on the effective thermal conductivity of open-cell foams, Chem. Eng. Process. - Process. Intensif. 129 (2018) 181–189, https://doi.org/10.1016/j.cep.2018.04.018.

[27] M.M. Yung, W.S. Jablonski, K.A. Magrini-Bair, Review of catalytic conditioning of biomass-derived syngas, Energy Fuels 23 (2009) 1874–1887, https://doi.org/10.1021/ef800830n.

[28] E. Fernandez, L. Santamaria, M. Artetxe, M. Amutio, A. Arregi, G. Lopez, J. Bilbao, M. Olazar, Conditioning the volatile stream from biomass fast pyrolysis for the attenuation of steam reforming catalyst deactivation, Fuel 312 (2022), 122910, https://doi.org/10.1016/j.fuel.2021.122910.

[29] P. Aghaei, C.G. Visconti, G. Groppi, E. Tronconi, Development of a heat transport model for open-cell metal foams with high cell densities, Chem. Eng. J. 321 (2017) 432–446, https://doi.org/10.1016/j.cej.2017.03.112.